A High-Precision Positioning Scheme Under Non-Point Visible Transmitters

Hongxiu Zhao, Jintao Wang, Xun Zhang, Bastien Béchadergue

Received 1 May 2020; revised 8 June 2020; accepted 19 June 2020. Date of publication 13 July 2020; date of current version 20 August 2020.
Digital Object Identifier 10.1109/OJCOMS.2020.3008340

A High-Precision Positioning Scheme Under Non-Point Visible Transmitters

HONGXIU ZHAO [1], JINTAO WANG [1] (Senior Member, IEEE), XUN ZHANG [2] (Senior Member, IEEE), AND BASTIEN BÉCHADERGUE [3]

[1] Department of Electronic Engineering, Tsinghua University, Beijing 10084, China
[2] LISITE Lab, Institute Supérieur d'Electronique de Paris, 92130 Paris, France
[3] Research and Development Department, Oledcomm, 78140 Vélizy-Villacoublay, France

CORRESPONDING AUTHOR: J. WANG (e-mail: wangjintao@tsinghua.edu.cn)

This work was supported in part by the Collaborative EU China Project funded by the National Key Research and Development Program of China under Grant 2017YFE011230, and in part by the Internet of Radio Light Project (IoRL) funded by European Union's Horizon 2020 Research and Innovation Program under Grant H2020-ICT 761992.

ABSTRACT An interacting multiple model based on unscented Kalman filter (IMM-UKF) is widely applied to positioning and tracking targets in various tracking scenarios. At the same time, visible light positioning (VLP) is developing rapidly due to the low cost and accuracy. Therefore, indoor positioning and tracking based on VLP combined with the IMM-UKF has attracted considerable interest. However, existing algorithms work on the assumption that the light-emitting diodes used for tracking are all point light sources, which ignores the geometry of these transmitters and results in low tracking accuracy. To overcome this problem, this paper proposes an innovative tracking algorithm based on VLP. This algorithm considers the shapes of the lights in combination with existing tracking algorithms, such as IMM-UKF. Simulation results show that in a standard Gaussian noise environment, the larger the transmitter is, the more meaningful the proposed algorithm is.

INDEX TERMS Target positioning and tracking, visible light positioning (VLP), interacting multiple model (IMM), unscented Kalman filter (UKF), shapes of transmitters.

I. INTRODUCTION

IN REAL-TIME target-tracking scenarios, a Kalman filter is widely applied as a linear quadratic estimation method due to its rapid convergence and low need for prior training [1]–[6]. It utilizes a great number of observed measurements, containing statistical noise and other inaccuracies, and computes unknown variables. To solve nonlinear tracking problems that may occur in reality, many kinds of improved Kalman filter have been proposed, including the extended Kalman filter (EKF), the unscented Kalman filter (UKF) and the cubature Kalman filter (CKF) [7]–[11]. In the EKF, the nonlinear observation and state models are linearized based on a first-order Taylor series expansion with the condition that the noise is deemed as Gaussian. Nevertheless, there is still instability caused by the model linearization and the numerous calculations of the Jacobian matrix that are required. The UKF is based on the unscented transform (UT) [7] and it makes a Gaussian approximation with a limited number of points, named Sigma points, to avoid the error caused by the first-order Taylor series expansion and the Jacobian matrix. A deterministic sampling approach is used to capture the mean and covariance estimates with a minimal set of samples, and the posterior mean and covariance undergoing a nonlinear propagation can be calculated accurately at least to the second order [8], [9]. The CKF is a special case of the UKF [10], [11]. Based on these filtering algorithms, interacting multiple model (IMM) can be constructed, including IMM-EKF and IMM-UKF [12]–[15]. In these IMM models, many kinds of movements can be considered and effectively integrated, which guarantees greater positioning accuracy. Because the less complexity and wide of applicability of UKF, IMM-UKF is adopted in this paper.

With high localization accuracy, visible light positioning (VLP) systems can be employed in numerous applications [16]–[25] with 5G. As for the signal acquisition,

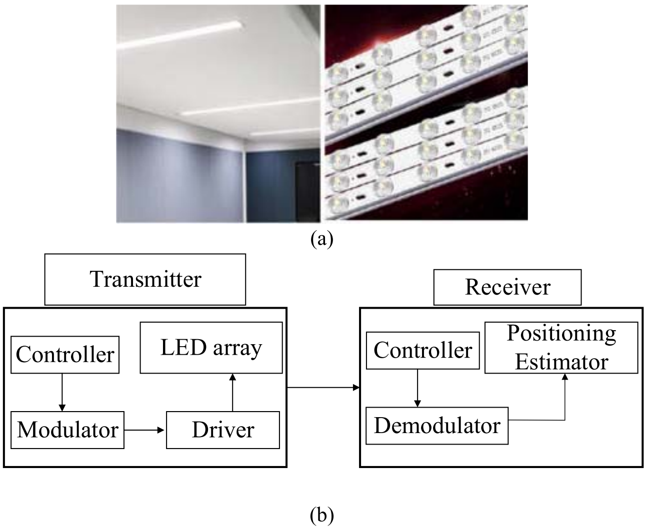

FIGURE 1. Common lights and architecture for VLP system.

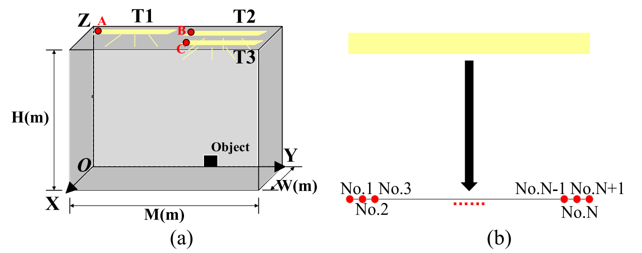

FIGURE 2. The scenario with common lights.

there exist lots of methods, including the widely applied Received Signal Strength (RSS), to receive the signals that include the typical identification (ID) information [26]–[29]. Obviously, all existing tracking methods based on VLP assume that the transmitter is the point located at the center of the light. However, there are some kinds of lights that are combined by LED array as shown in Fig. 1 (a) and the ID information with f_i frequency from each light is transmitted from the whole light plane (LED array) rather than from the center point of the light. The classical architecture for a simple VLP system is as shown in Fig. 1 (b) and each transmitter is composed of LED array. As for RSS algorithm, the power of the received signal is inversely proportional to the square of the distance between the receiver and the transmitter [29], so a small distance difference can cause a great attenuation or increase of the received signal power. Therefore, the choice of the equivalent transmitter point of the light is particularly critical. Since most of the received power comes from the power of the nearest point of the light, it is suitable to consider the nearest point of the light to the target rather than the center point as the transmitter point. Especially in a relatively small room, ignoring the shapes of the lights causes significant errors in the tracking system and the calculated path. This is because the larger the room is, the more closely the lights will approximate to particles and the more the nearest point of the light to the target can be equivalent to the center of the light. Therefore, in this paper, to correct the errors caused by the signal acquisition, a high-accuracy tracking algorithm is proposed and simulated based on the shapes of lights with a focus on practical utility.

II. SYSTEM MODEL

To explain the proposed algorithm concisely, a classic scenario is adopted in this paper, as shown in Fig. 2(a). The parameters M, W and H are the length, width and height of the room, respectively. As mentioned in Section I, the shapes of the lights are noticeable and significant. Although there are lights of various geometric shapes, the most common shape is the rectangle. Thus, rectangular lights (T1, T2, T3) are considered in this paper. These lights are used to transmit synchronized information and locate an object. The coordinate system is arranged as shown in Fig. 2 (a). In most scenarios, the length of the lights is much greater than their width. Therefore, each light can be regarded as a line, as shown in Fig. 2 (b). Furthermore, each light can be considered as being equivalent to a collection of multiple points. Each light is therefore divided into N segments, resulting in $N + 1$ points as shown in Fig. 2 (b).

III. THE PROPOSED ALGORITHM

There are two steps in the proposed algorithm. As past researches and existing applications have shown, the positioning of a target can be calculated using the RSS algorithm. However, the measurement is inaccurate because the traditional RSS algorithm ignores the shapes of the lights, random noise occurs during signal transmission and there are many kinds of disturbances. Therefore, the first step in the proposed algorithm is to weaken the influence of the shapes of the lights. In the second step, the positioning and tracking errors caused by random noise are reduced by using IMM-UKF. The details are expanded as follows.

A. FIRST STEP: UPDATED MEASUREMENTS BASED ON THE SHAPES OF THE LIGHTS

According to the principles of the traditional RSS algorithm, the positioning accuracy depends not only on the distances d_i, $(i = 1, 2, 3)$ between each light (T1, T2, T3) and the target, but also on the position of each light (x_i, y_i, z_i). Therefore, positioning and tracking errors are caused by the inaccuracy of these parameters. Because the error of the measured distance d_i, which is caused by the transmission noise under LOS, can be decreased by filters, this section focuses on the correction of the position of each light (x_i, y_i).

In the traditional RSS algorithm, the position of the center point of the light is regarded as the position of the transmitter (x_i, y_i) with the assumption that the measured distance d_i is the distance between the receiver and the center of the light. The measured distance d_i is calculated according to the power at transmitter side P_{ti} and the power at receiver side P_{ri}. However, P_{ri} comes from the whole light, not the center point of the light. Therefore, it is essential to find out the ideal transmitting point.

Because P_{ri} is inversely proportional to the square of the distance between the transmitting point and receiver, the further the transmitting point of the light is from the receiver, the less contribution to P_{ri}. Given that there are two points (a, b) on a light in the classical room, and the distance between each point and the target to be positioned is d_a and d_b, respectively, the received power from the first point is $(d_b/d_a)^4$ of the second one according to the Lambertian irradiation pattern. If the two points are the center point and the nearest point to the target, respectively, the distance d_{ab} between them may be about $L/2$ where L is the length of the light. Obviously, $d_a - d_{ab} \leq d_b \leq d_a$, therefore, d_b may be around $(d_a - d_{ab} + d_a)/2$ and d_b/d_a may be 1-$d_{ab}/(2d_a)$ during the movement of the receiver. Assuming a common scenario, $L = 1/10 \cdot d_a$, therefore, d_b/d_a can be 1-$d_{ab}/(20L)$ and $(d_b/d_a)^4$ is around 90% which means that the receiver could receive 11% more power from b point than from a point. Therefore, the ideal transmitting point is the nearest point b, rather than the middle position of the light. With the help of the nearest point to the receiver, the preliminary result calculated by the traditional RSS algorithm can be updated to have increased accuracy. The details of this procedure are as follows.

Initially, the traditional algorithm is applied and a preliminary result is determined. In the process of RSS signal propagation under VLP, the Lambertian irradiation pattern is used to model the transmitter performance in the indoor line of sight (LOS) channels [30]. The power of the received signal with frequency f_i in this model is expressed as (1).

$$P_{ri} = \frac{m+1}{2\pi {d_i}^2} \cdot D \cdot \cos(\varphi_i)^m \cdot \cos(\psi_i) \cdot P_{ti}, \quad i = 1, 2, 3 \quad (1)$$

where m is the order of Lambertian emission and usually linked to the semi-angle at half power $\phi_{1/2}$ with $m = -ln2/ln(cos\phi_{1/2})$. If $\phi_{1/2} = 60°$, then $m = 1$. D is the physical area of the receiver. d_i is the distance between the receiver and the transmitter carrying the f_i frequency. ϕ_i is the irradiation angle and ψ_i is the incident angle. P_{ti} is the power of the transmitted signal. If the receiver (PD) plane is parallel to the transmitter (light) plane, ϕ and ψ can be set as

$$\varphi_i = \psi_i = arccos\frac{H}{d_i}, \quad i = 1, 2, 3 \quad (2)$$

(1) can be simplified to

$$P_{ri} = P_{ri,0}\left(\frac{d_{i,0}}{d_i}\right)^4 \quad (3)$$

where $P_{ri,0}$ is the received power from the i_{th} transmitter at a reference distance $d_{i,0}$ away from that transmitter. However, the order of Lambertian emission in (2) is not 1 for nonideal LED and PDs [31]–[34]. Therefore, the path loss exponent in (3) is not 4. It can be estimated from the

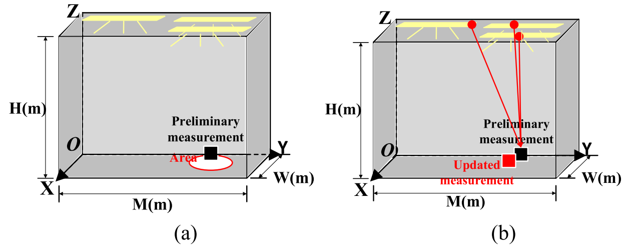

FIGURE 3. Update process.

offline measurements and (3) can be generalized as

$$P_{ri} = P_{ri,0}\left(\frac{d_{i,0}}{d_i}\right)^{TL_i} \quad (4)$$

$$TL_i = log\left(\frac{P_{ri}}{P_{ri,0}}\right)/log\left(\frac{d_{i,0}}{d_i}\right) \quad (5)$$

Therefore, the distance d_i can be measured. At the same time, the transmitted power P_{ti} is assumed to be emitted by the center point of the light, therefore, the position of the transmitter (x_i, y_i, z_i) used in (4) is the position of the center with $z = 0$.

$$d_i = \sqrt{(x - x_i)^2 + (y - y_i)^2 + (z - z_i)^2} \quad (6)$$

Based on the center point of the light, the position of the target is calculated as follows.

$$\boldsymbol{A} \cdot X = b \quad (7)$$

where $\boldsymbol{A} = 2 \cdot \begin{bmatrix} x_1 - x_2 & y_1 - y_2 \\ x_1 - x_3 & y_1 - y_3 \end{bmatrix}$, $X = \begin{bmatrix} x \\ y \end{bmatrix}$ and $b = \begin{bmatrix} {d_{xy2}}^2 - {d_{xy1}}^2 + {x_1}^2 - {x_2}^2 + {y_1}^2 - {y_2}^2 \\ {d_{xy3}}^2 - {d_{xy1}}^2 + {x_1}^2 - {x_3}^2 + {y_1}^2 - {y_3}^2 \end{bmatrix}$.

According to Fig. 2 (a), $\boldsymbol{A}$ is an invertible matrix. Based on the traditional RSS algorithm discussed above, the preliminary result is obtained from the following equation.

$$X = \boldsymbol{A}^{-1} \cdot b \quad (8)$$

If there is a tilt, the way in [16] can be used to obtain the irradiation angle ϕ_i and the incident angle ψ_i with $\psi_i = \phi_i - \theta$ where θ is the orientation angle. Therefore, the 2D positioning X can be calculated. In this work, to clarify the significance of the shape of lights in VLC and simplify the system model, it is assumed that the transmitter is parallel to the receiver.

Next, we update the preliminary result. Because the position of each light (x_i, y_i) used above is not accurate, as discussed in the previous section, the preliminary result is not accurate either. Although the preliminary measurement needs to be updated, the approximate area of the target can be determined as shown in Fig. 3 (a). To obtain a more accurate measurement, it is necessary to correct the position of each light in the RSS algorithm with the help of the approximate range.

As discussed above, the transmitted power P_{ti} comes from the whole light. However, as the transmitting point of the light gets farther and farther away from the receiver, the power it contributes is greatly reduced, which means that it is better to think of d_i as the distance between the receiver and the nearest point of the light to the target, not the center point. Therefore, divide the light into N segments as shown in Fig. 2 (b), producing N+1 positions in total. The distances between all the positions of each light and the preliminary result can be calculated.

$$d_{i,k} = \sqrt{\left(x - x_{i,k}\right)^2 + \left(y - y_{i,k}\right)^2},\ \ k = 1, 2, \ldots\ldots N + 1 \tag{9}$$

where (x, y) is the preliminary measurement and $(x_{i,k}, y_{i,k})$ is the k_{th} position of the i_{th} light. By comparing these distances, the minimum distance $d_{i,kmin}$ is found. The nearest position $(x_{i,kmin}, y_{i,kmin})$ of each light to the preliminary measurement, which generates the minimum distance $d_{i,kmin}$ can also be determined, as shown in Fig. 3 (b). Then, the position $(x_{i,kmin}, y_{i,kmin})$ of each light is substituted into (6)-(8). This process corrects the position of each light. An updated measurement (x, y) is then calculated according to (6)-(8).

The updated measurement is more accurate than the preliminary measurement. However, the position of the light $(x_{i,kmin}, y_{i,kmin})$ is the nearest position to the preliminary measurement, not to the target. Furthermore, the updated measurement is based on the preliminary measurement. This updated measurement is still not precise enough. Therefore, it is necessary to further update the updated measurement. Specifically, in the same way that the preliminary result was updated, the updated measurement (x, y) is substituted into (9) again to calculate the distances $d_{i,k}$ between the measurement and the N + 1 positions of each light. Then, these distances are compared to find the minimal distance among them. The nearest position of each light to the updated measurement can also be determined. These new nearest positions can then be substituted into (7) and (8) again to calculate a more precise measurement of (x, y).

In this update process with an increasing number of iterations, the nearest position of each light to the measurement result tends further toward the nearest position to the real target, and the measurement result hence becomes increasingly accurate.

B. SECOND STEP: INTERACTING MULTIPLE MODEL-UNSCENTED KALMAN FILTER

Consider the measurement result calculated in the previous part as $z = (x, y)^T$. The state vector at time k of the target at time k is X_k. $X_k = (x, x_v, y, y_v)^T$, where (x, y) is the real-time position of the target and (x_v, y_v) is the speed of the target along the X and Y axes. Two axes in the coordinate system are set as shown in Fig. 2 (a). The state equation and measurement equations are given, respectively.

$$X_k = f(X_{k-1}) + w_{k-1} \tag{10}$$

$$z = h(X_k) + v_k \tag{11}$$

where w_k and v_k are the process noise and measurement noise, respectively. It is assumed that these two kinds of noise are both Gaussian, and $\boldsymbol{Q}_k = E[w_k \cdot {w_k}^T]$, $\boldsymbol{R}_k = E[v_k \cdot {v_k}^T]$.

1) KINEMATIC MODELS

To describe the movement of the target more precisely, the kinematic model of the target involves the interaction by multiple models. Two practical and typical models are considered, the constant velocity (CV) and coordinated turn (CT) models. The state equation and measurement equation are simplified.

$$X_k = \boldsymbol{A} \cdot X_{k-1} + w_{k-1} \tag{12}$$

$$z = \boldsymbol{H} \cdot X_k + v_k \tag{13}$$

where $\boldsymbol{A}$ is the state transition matrix, which changes with the motion model of the target, and $\boldsymbol{H}$ is the observation matrix, $\boldsymbol{H} = \begin{bmatrix} 1 & 0 & 0 & 0 \\ 0 & 0 & 1 & 0 \end{bmatrix}$.

The first model is the CV model. In this model, the speed of the target is fixed and the state transition matrix is:

$$\boldsymbol{A} = \begin{bmatrix} 1 & \Delta t & 0 & 0 \\ 0 & 1 & 0 & 0 \\ 0 & 0 & 1 & \Delta t \\ 0 & 0 & 0 & 1 \end{bmatrix} \tag{14}$$

where Δt is the interval between adjacent states.

The second model is the CT model. When the state of the target is a four-dimensional vector, the state transition matrix is as depicted.

$$\mathbf{A} = \begin{bmatrix} 1 & \frac{\sin(\omega \Delta t)}{\omega} & 0 & \frac{\cos(\omega \Delta t) - 1}{\omega} \\ 0 & \cos(\omega \Delta t) & 0 & -\sin(\omega \Delta t) \\ 0 & \frac{1 - \cos(\omega \Delta t)}{\omega} & 1 & \Delta t \\ 0 & \sin(\omega \Delta t) & 0 & \cos(\omega \Delta t) \end{bmatrix} \tag{15}$$

Here, the constant parameter ω is the angular rate and represents the coupling effect between the X axis and Y axis.

2) UNSCENTED KALMAN FILTER

As mentioned in Section I, the UKF can address noise problems in a nonlinear system using a set of Sigma points. The mean and variance of the state at time k can be calculated more precisely using the Sigma points. The details of the standard UKF are as follows.

Firstly, initialize the state and covariance matrices of the target as $\hat{X}_0$ and $\boldsymbol{P}_0$, respectively.

$$\hat{X}_0 = E[\mathrm{X}_0] \tag{16}$$

$$\boldsymbol{P}_0 = E\left[\left(X_0 - \hat{X}_0\right)\left(X_0 - \hat{X}_0\right)^T\right] \tag{17}$$

Secondly, as described in the unscented transformation, 2N + 1 Sigma points need to be calculated using (18), where N is the number of dimensions of state X_{k-1}. The set of Sigma points is $\boldsymbol{\chi}_{k-1}$.

$$\boldsymbol{\chi}_{k-1,n} = \begin{cases} \hat{X}_{k-1}, & n = 0 \\ \hat{X}_{k-1} + \left(\sqrt{(N+\kappa)(\mathbf{P}_{k-1})_n}\right), & n = 1, \ldots, N \\ \hat{X}_{k-1} - \left(\sqrt{(N-\kappa)(\mathbf{P}_{k-1})_n}\right), & n = N+1, \ldots, 2N \end{cases} \tag{18}$$

where $(\cdot)_n$ is n_{th} column of matrix $(\cdot)$. κ is adjustable and $\kappa = \alpha^2(N+\lambda)-N$. α determines the distribution of Sigma points and it is usually set between e^{-4} and 1. As a constant parameter, the value of λ is generally 0 or 3-N.

Thirdly, the predicted state of the target is updated to obtain $\boldsymbol{X}_{k|k-1}$ and its mean and covariance matrices are calculated.

$$\boldsymbol{X}_{k|k-1} = f(\boldsymbol{\chi}_{k-1}) \tag{19}$$

$$\overline{X}_{k|k-1} = \sum_{n=0}^{2N} \omega_n^m (\boldsymbol{X}_{k|k-1})_n \tag{20}$$

$$\boldsymbol{P}_{k|k-1} = \sum_{n=0}^{2N} \omega_n^c [(\boldsymbol{X}_{k|k-1})_n - \overline{X}_{k|k-1}] \times [(\boldsymbol{X}_{k|k-1})_n - \overline{X}_{k|k-1}]^T + \boldsymbol{Q}_k \tag{21}$$

where $(\boldsymbol{X}_{k|k-1})_n$ refers to the nth column of the matrix $\boldsymbol{X}_{k|k-1}$ and w^m is the weight of each Sigma point obtained according to (22). Similarly, w^c is the weight of each Sigma point related to the covariance matrix and is obtained according to (23). In this equation, when the distribution of X_k is Gaussian distribution according to the prior knowledge, the best value for β is 2.

$$\omega_n^m = \begin{cases} \frac{\kappa}{\kappa+N}, & n = 0 \\ \frac{\kappa}{2(\kappa+N)}, & n = 1, \dots, 2N \end{cases} \tag{22}$$

$$\omega_n^c = \begin{cases} \frac{\kappa}{\kappa+N} + (1-\alpha^2+\beta), & n = 0 \\ \frac{\kappa}{2(\kappa+N)}, & n = 1, \dots, 2N \end{cases} \tag{23}$$

Next, calculate the Sigma points of $\overline{X}_{k|k-1}$ as $\boldsymbol{\chi}_k$ and update the observation $z_{k|k-1}$.

$$\boldsymbol{\chi}_{k,n} = \begin{cases} \overline{X}_{k|k-1}, & n = 0 \\ \overline{X}_{k|k-1} + \left(\sqrt{(N+\kappa)(\mathbf{P}_{k|k-1})_n}\right), & n = 1, \dots, N \\ \overline{X}_{k|k-1} - \left(\sqrt{(N-\kappa)(\mathbf{P}_{k|k-1})_n}\right), & n = N+1, \dots, 2N \end{cases} \tag{24}$$

The mean and covariance matrix can be obtained as well.

$$z_{k|k-1} = h(\boldsymbol{\chi}_k) \tag{25}$$

$$\overline{z}_{k|k-1} = \sum_{n=0}^{2N} \omega_n^m (z_{k|k-1})_n \tag{26}$$

$$\boldsymbol{P}_{z_k} = \sum_{n=0}^{2N} \omega_n^c [\overline{z}_{k|k-1} - (z_{k|k-1})_n] \times [\overline{z}_{k|k-1} - (\mathbf{z}_{k|k-1})_n]^T + \boldsymbol{R}_k \tag{27}$$

$$\boldsymbol{P}_{X_k z_k} = \sum_{n=0}^{2N} \omega_n^c [(\mathbf{X}_{k|k-1})_n - \overline{X}_{k|k-1}] \times [\overline{z}_{k|k-1} - (z_{k|k-1})_n]^T \tag{28}$$

The gain of the state $\boldsymbol{K}_k$ is calculated.

$$\boldsymbol{K}_k = \boldsymbol{P}_{X_k z_k} {\boldsymbol{P}_{z_k}}^{-1} \tag{29}$$

Finally, the best estimate at time k is updated.

$$\hat{X}_k = \overline{X}_{k|k-1} + \boldsymbol{K}_k (z_k - z_{k|k-1}) \tag{30}$$

$$\boldsymbol{P}_k = \boldsymbol{P}_{k|k-1} - \boldsymbol{K}_k \boldsymbol{P}_k \boldsymbol{K}_k^T \tag{31}$$

where z_k is the measurement calculated in part A.

3) INTERACTING MULTIPLE MODEL WITH UKF

As mentioned in Section I, an interacting multiple-model UKF is useful for real-time positioning and tracking, and is applicable for a system with an uncertain noise distribution. Three stages, interaction, filtering and combination, will be introduced based on the UKF described previously. Here are the specific details under the assumption that there are L models and the initial probability of each model is μ_0^j, $j = 1, \dots, L$, corresponding to the state of each model. The parameter π_{ij} denotes the possibility of a transition from the i_{th} model to the j_{th} model.

The system is initialized with $\hat{X}_0^j$ and the covariance matrix $\boldsymbol{P}_0^j$ corresponding to the j_{th} model. In the interaction stage, the interactive value of each model is calculated.

$$\hat{X}_{k-1}^{0j} = \sum_{i=1}^{L} \mu_{k-1}^{ij} \hat{X}_{k-1}^i \tag{32}$$

$$\mu_{k-1}^{ij} = \frac{\pi_{ij}\mu_{k-1}^j}{\overline{c}_j} \tag{33}$$

$$\overline{c}_j = \sum_{i=1}^{L} \pi_{ij}\mu_{k-1}^j \tag{34}$$

$$\boldsymbol{P}_{k-1}^{0j} = \sum_{i=1}^{L} \mu_{k-1}^{ij} \left[\boldsymbol{P}_{k-1}^i - \left(\hat{X}_{k-1}^{0j} - \hat{X}_{k-1}^i\right)\left(\hat{X}_{k-1}^{0j} - \hat{X}_{k-1}^i\right)^T\right] \tag{35}$$

In the filtering stage, $\hat{X}_{k-1}^j$ and the previously obtained covariance matrix $\boldsymbol{P}_{k-1}^j$ are used as the inputs of the UKF. Then, as described in the previous part, the best estimate $\hat{X}_k^j$ and the covariance matrix $\boldsymbol{P}_{k-1}^j$ of the j_{th} model at time k can be calculated. In the combination stage, the interactive best estimate $\hat{X}_k$ and the covariance matrix $\boldsymbol{P}_k$ can be calculated.

$$\Lambda_k^j = \frac{1}{\sqrt{2\pi \left|\boldsymbol{S}_k^j\right|}} e^{-\frac{1}{2} d_j^T \left(\boldsymbol{S}_k^j\right)^{-1} d_j} \tag{36}$$

where $\boldsymbol{S}_k^j = \boldsymbol{H}\boldsymbol{P}_{k|k-1}^j\boldsymbol{H}^T + \boldsymbol{R}_k$ and $d_j = z_k^j - \boldsymbol{H}\overline{X}_{k|k-1}^j$.

$$\mu_{k-1}^j = \frac{\Lambda_k^j \sum_{i=1}^{L} \mu_{k-1}^j \pi_{ij}}{c} \tag{37}$$

where $c = \sum_{i=1}^{l} \Lambda_k^j \overline{c}_j$.

$$\hat{X}_k = \sum_{j=1}^{L} \mu_k^j \hat{X}_k^j \tag{38}$$

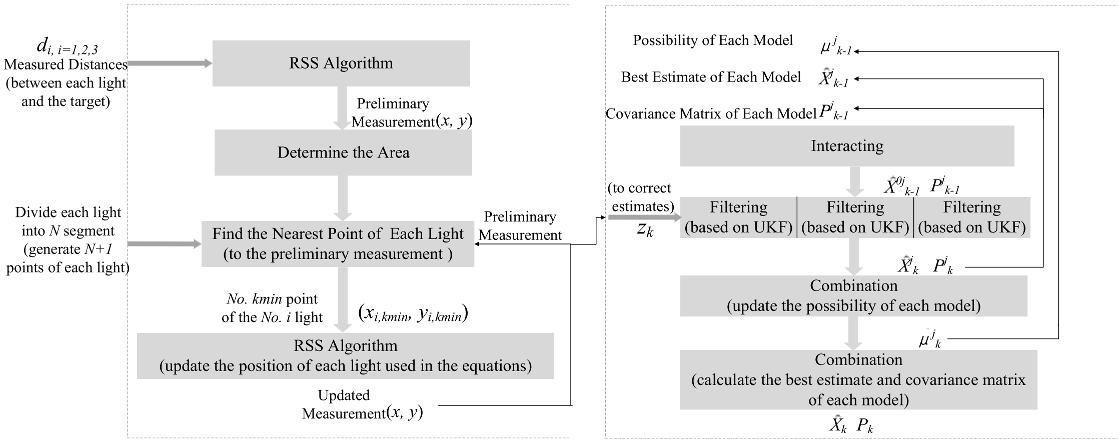

FIGURE 4. Overview of the process.

$$\boldsymbol{P}_k = \sum_{j=1}^{L} \mu_k^j \left[\boldsymbol{P}_{k-1}^j - \left(\hat{X}_k - \hat{X}_k^j \right) \left(\hat{X}_k - \hat{X}_k^j \right)^T \right] \tag{39}$$

From the previous parts, the measurement is calculated and updated based on the shape of the light, the updated measurement is then used to correct the estimates using the IMM-UKF. Finally, the corrected estimate value is determined with the assumption that there are three lights and the positions of all points generated from dividing each light (T1, T2, T3) are already known. The overall scheme is shown in Fig. 4.

IV. NUMERICAL RESULTS

A. RESULTS WITH DIFFERENT ALGORITHM

Simulations were conducted with the assumption that $M = 18$m, $W = 12$m, $H = 4$m with the origin defined as (0, 0). In addition, $N = 200$, indicating that each light is divided into 200 segments, creating 201 points. The starting points (A, B, C) of the three lights are at (400, 300), (1400, 300) and (1400, 900), respectively, as shown in Fig. 2 (a). The length of each light is 100cm. The path loss exponent in (4) can be set as 4.17, 4.18 and 4.21 [29] corresponding to three lights, respectively.

It is assumed that the position of the target is sampled every 0.5 seconds with one step. Periods of acceleration are likely to be short and uniform. Therefore, in the application of these models, only the CV and CT cases are considered. The target starts from the coordinate (100, 100) with a speed of 25cm/s along the X and -65cm/s along the Y axis. After 20 steps, it turns left with angular velocity 10rad/s. Then, after another 20 steps, it turns right with angular velocity -10rad/s. Therefore, in the simulations, the first case is CV, the second case is CT with $w > 0$ and the third case is CT with $w < 0$.

As shown in Fig. 5, the high performance of the proposed algorithm is demonstrated. The tracking path calculated by the traditional RSS algorithm ignoring the shapes of the lights deviates from the real path. However, the path calculated by the proposed tracking algorithm almost coincides

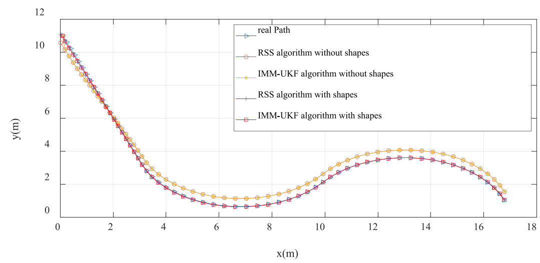

FIGURE 5. Real path of the target and paths calculated by several algorithms.

with the actual path, which indicates the importance of considering the shapes of the lights. Fig. 6 (a) shows the positioning and tracking root mean square error (RMSE) calculated from the paths generated by the different algorithms. To see the slight difference between two adjacent lines, Fig. 6 (b) shows lines from the top of Fig. 6 (a). The first line is calculated based on the traditional RSS algorithm without considering the shapes of the lights, and the second one is obtained from the traditional IMM-UKF algorithm. Both of lines show an RMSE of around 0.4m. Two lines in Fig. 6 (c) include the consideration of the shapes of the lights and show an RMSE of around 30mm RMSE. The large RMSE difference between Fig. 6 (b) and Fig. 6 (c) indicates the significance of considering the shapes of the lights. It is worth noting that there are still slight differences between the lines in each of two pairs, which indicates the necessity of IMM-UKF algorithm.

The importance of considering shapes of the lights is also expounded from the perspective of the possibility of each motion model in Fig. 7. There are two possibility results of the models in each graph, one calculated using the proposed algorithm considering the shapes of the lights and the other one calculated by the algorithm without considering the shapes of the lights. The possibility of each model should be 1 during times when it is working and 0 when other models work. Considering the possibilities of the three models, the proposed algorithm which considers the shapes of the light is better than models not considering the shapes of the lights.

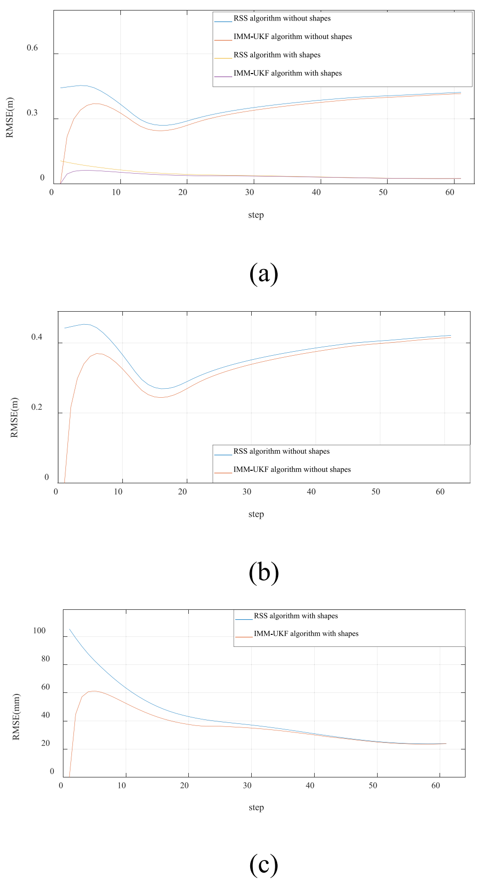

FIGURE 6. The tracking errors calculated several algorithms.

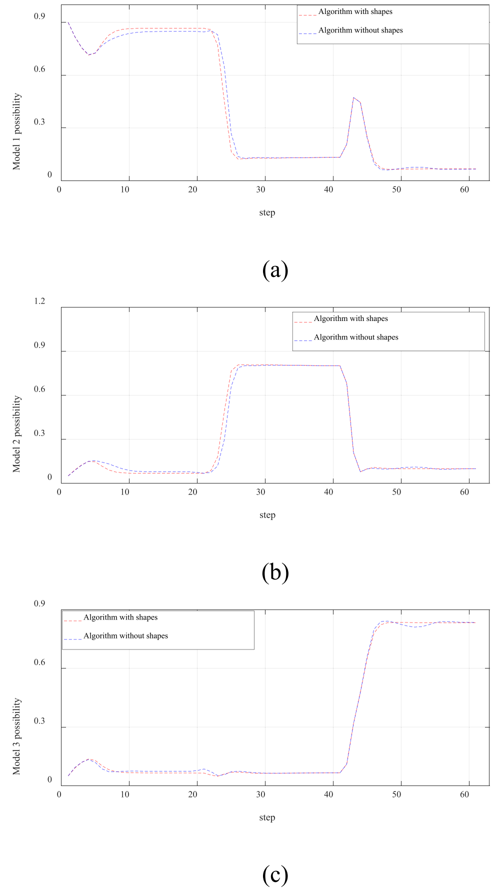

FIGURE 7. Possibilities of each model based on different algorithms.

B. RESULTS WITH DIFFERENT UPDATES

The proposed algorithm is essentially an update algorithm. Therefore, it is necessary to find the best number of updates. Set the length of each transmitter to 1m, which is the same as the previous part. As shown in Fig. 8 (a), the RMSE of the algorithm is 40mm after 1 update, but the RMSE remains stable at 20mm after 2 updates. Fig. 8 (b) explains the necessity of updating from the perspective of cumulative distribution function (CDF), which also proved the optimal update time is 2 in this case.

In another case, the length of the transmitter is 1.5m, as shown in Fig. 9. In this case, the RMSE is 600mm after 1 update and 60mm after 2 updates, indicating that the optimal number of updates in this case is the same as the previous case. It is believed that, no matter how long the light is, the limited number of updates in the proposed algorithm is sufficient to make the error converges steadily, and in this simulation scheme, the error converges to about 60mm.

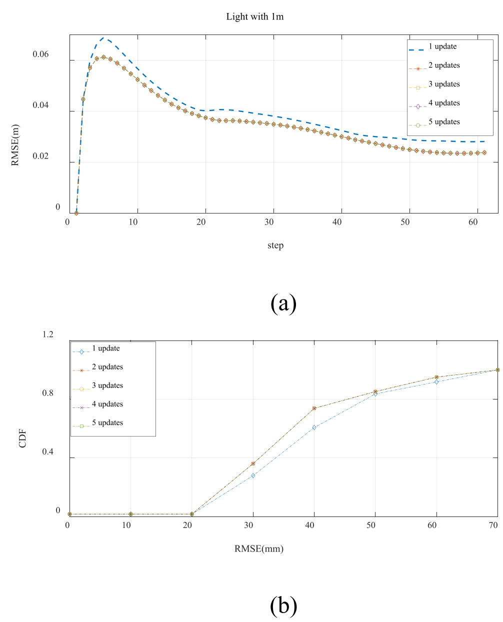

FIGURE 8. Positioning and tracking errors after k updates with 1mm transmitters.

C. RESULTS WITH DIFFERENT TRANSMITTERS

The previous part determined the optimal number of updates, therefore, to illustrate the significance of the shapes of the lights further and verify the convergence of the algorithm, simulations shows the results of the algorithm after 2 updates for two kinds of lights. The lengths of lights are 1m or 1.5m, respectively and CDF is shown in Fig. 10. There is a slight difference between the two cases, which demonstrates the algorithm is more effective in reducing the error caused by

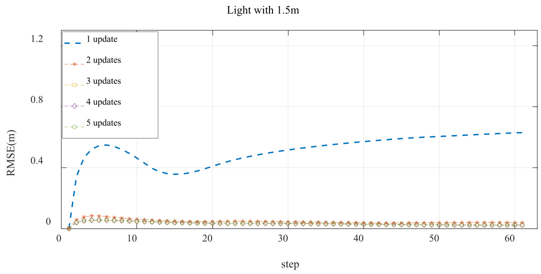

(a)

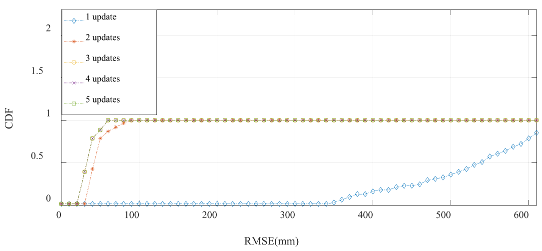

(b)

FIGURE 9. **Positioning and tracking errors after k updates with 1.5mm transmitters.**

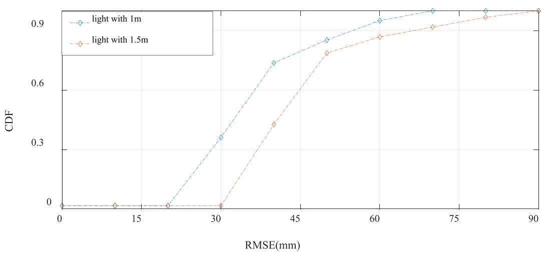

FIGURE 10. **Positioning and tracking errors caused by two different lights after 2 updates.**

the light with a length of 1.5m, but it can be noticed that the blue line converges to 1 before the red line, which means that although the proposed algorithm works well, the smaller transmitter is a better choice.

V. CONCLUSION

In this paper, an innovative positioning and tracking algorithm was proposed based on VLP. Considering the shapes of the transmitters (lights), the positioning error of the proposed algorithm was found to be much lower than that of the traditional algorithms. Compared with the error caused by the traditional IMM-UKF algorithm, there is a reduction of 96% under the proposed algorithm in the simulation. However, different positions of lights in the room and different divisions of each light could lead to different tracking results. Further research needs to be conducted to examine these factors.

REFERENCES

[1] Y. Zhao, "Cubature + extended hybrid kalman filtering method and its application in PPP/IMU tightly coupled navigation systems," *IEEE Sensors J.*, vol. 15, no. 12, pp. 6973–6985, Dec. 2015.

[2] G. Du, G. Yao, C. Li, and P. X. Liu, "Natural human–robot interface using adaptive tracking system with the unscented Kalman filter," *IEEE Trans. Human-Mach. Syst.*, vol. 50, no. 1, pp. 42–54, Feb. 2020.

[3] Y. Liu, S. Li, Q. Fu, Z. Liu, and Q. Zhou, "Analysis of Kalman filter innovation-based GNSS spoofing detection method for INS/GNSS integrated navigation system," *IEEE Sensors J.*, vol. 19, no. 13, pp. 5167–5178, Jul. 2019.

[4] D. Cichon, R. Psiuk, H. Brauer, and H. Töpfer, "A hall-sensor-based localization method with six degrees of freedom using unscented Kalman filter," *IEEE Sensors J.*, vol. 19, no. 7, pp. 2509–2516, Apr. 2019.

[5] Y. Huang and Y. Zhang, "A new process uncertainty robust student's t based Kalman filter for SINS/GPS integration," *IEEE Access*, vol. 5, pp. 14391–14404, 2017.

[6] J. Yin, R. Tiwari, and M. Johnston, "Robust GPS carrier tracking model using unscented Kalman filter for a dynamic vehicular communication channel," *IEEE Access*, vol. 6, pp. 26930–26938, 2018.

[7] S. J. Julier and J. K. Uhlmann, "Unscented filtering and nonlinear estimation," *Proc. IEEE*, vol. 92, no. 3, pp. 401–422, Mar. 2004.

[8] X. Ning, F. Wang, and J. Fang, "An implicit UKF for satellite stellar refraction navigation system," *IEEE Trans. Aerosp. Electron. Syst.*, vol. 53, no. 3, pp. 1489–1503, Jun. 2017.

[9] Y. Liu, H. Wang, and C. Hou, "UKF based nonlinear filtering using minimum entropy criterion," *IEEE Trans. Signal Process.*, vol. 61, no. 20, pp. 4988–4999, Oct. 2013.

[10] F. Sandblom and L. Svensson, "Moment estimation using a marginalized transform," *IEEE Trans. Signal Process.*, vol. 60, no. 12, pp. 6138–6150, Dec. 2012.

[11] I. Arasaratnam and S. Haykin, "Cubature Kalman filters," *IEEE Trans. Autom. Control*, vol. 54, no. 6, pp. 1254–1269, Jun. 2009.

[12] D. Lee, C. Liu, Y. Liao, and J. K. Hedrick, "Parallel interacting multiple model-based human motion prediction for motion planning of companion robots," *IEEE Trans. Autom. Sci. Eng.*, vol. 14, no. 1, pp. 52–61, Jan. 2017.

[13] S. J. Lee, Y. Motai, and H. Choi, "Tracking human motion with multichannel interacting multiple model," *IEEE Trans. Ind. Informat.*, vol. 9, no. 3, pp. 1751–1763, Aug. 2013.

[14] A. O. Abdul Salam, R. E. Sheriff, Y. Hu, S. R. Al-Araji, and K. Mezher, "Automatic modulation classification using interacting multiple model Kalman filter for channel estimation," *IEEE Trans. Veh. Technol.*, vol. 68, no. 9, pp. 8928–8939, Sep. 2019.

[15] L. Hong, "Multirate interacting multiple model filtering for target tracking using multirate models," *IEEE Trans. Autom. Control*, vol. 44, no. 7, pp. 1326–1340, Jul. 1999.

[16] M. Yasir, S. Ho, and B. N. Vellambi, "Indoor positioning system using visible light and accelerometer," *J. Lightw. Technol.*, vol. 32, no. 19, pp. 3306–3316, Oct. 1, 2014.

[17] X. Zhang, J. Duan, Y. Fu, and A. Shi, "Theoretical accuracy analysis of indoor visible light communication positioning system based on received signal strength indicator," *J. Lightw. Technol.*, vol. 32, no. 21, pp. 4180–4186, Nov. 1, 2014.

[18] M. F. Keskin and S. Gezici, "Comparative theoretical analysis of distance estimation in visible light positioning systems," *J. Lightw. Technol.*, vol. 34, no. 3, pp. 854–865, Feb. 01, 2016.

[19] W. Gu, M. Aminikashani, P. Deng, and M. Kavehrad, "impact of multipath reflections on the performance of indoor visible light positioning systems," *J. Lightw. Technol.*, vol. 34, no. 10, pp. 2578–2587, May 15, 2016.

[20] M. F. Keskin, E. Gonendik, and S. Gezici, "Improved lower bounds for ranging in synchronous visible light positioning systems," *J. Lightw. Technol.*, vol. 34, no. 23, pp. 5496–5504, Dec. 1, 2016.

[21] H. Steendam, T. Q. Wang, and J. Armstrong, "Theoretical lower bound for indoor visible light positioning using received signal strength measurements and an aperture-based receiver," *J. Lightw. Technol.*, vol. 35, no. 2, pp. 309–319, Jan. 15, 2017.

[22] J. Armstrong, Y. A. Sekercioglu, and A. Neild, "Visible light positioning: A roadmap for international standardization," *IEEE Commun. Mag.*, vol. 51, no. 12, pp. 68–73, Dec. 2013.

[23] L. Shi *et al.*, "5G Internet of radio light positioning system for indoor broadcasting service," *IEEE Trans. Broadcast.*, vol. 66, no. 2, pp. 534–544, Jun. 2020.

[24] L. Shi *et al.*, "Experimental testbed for VLC-based localization framework in 5G Internet of radio light," in *Proc. 26th IEEE Int. Conf. Electron. Circuits Syst.*, Genoa, Italy, 2019, pp. 430–433.
[25] J. Cosmas *et al.*, "5G Internet of radio light services for Musée de la Carte à Jouer," in *Proc. Global LIFI Congr.*, Paris, France, 2018, pp. 1–6.
[26] M. H. Bergen, X. Jin, D. Guerrero, H. A. L. F. Chaves, N. V. Fredeen, and J. F. Holzman, "Design and implementation of an optical receiver for angle-of-arrival-based positioning," *J. Lightw. Technol.*, vol. 35, no. 18, pp. 3877–3885, Sep. 15, 2017.
[27] D.-H. Shin and T.-K. Sung, "Comparisons of error characteristics between TOA and TDOA positioning," *IEEE Trans. Aerosp. Electron. Syst.*, vol. 38, no. 1, pp. 307–311, Jan. 2002.
[28] A. Booranawong, N. Jindapetch, and H. Saito, "Adaptive filtering methods for RSS signals in a device-free human detection and tracking system," *IEEE Syst. J.*, vol. 13, no. 3, pp. 2998–3009, Sep. 2019.
[29] Q. Luo, Y. Peng, J. Li, and X. Peng, "RSS-based localization through uncertain data mapping for wireless sensor networks," *IEEE Sensors J.*, vol. 16, no. 9, pp. 3155–3162, May 2016.
[30] S. Zhang, P. Du, C. Chen, W. Zhong, and A. Alphones, "Robust 3D indoor VLP system based on ANN using hybrid RSS/PDOA," *IEEE Access*, vol. 7, pp. 47769–47780, 2019.
[31] Y. Zhuang *et al.*, "A survey of positioning systems using visible LED lights," *IEEE Commun. Surveys Tuts.*, vol. 20, no. 3, pp. 1963–1988, 3rd Quart., 2018.
[32] F. Alam, M. T. Chew, T. Wenge, and G. S. Gupta, "An accurate visible light positioning system using regenerated fingerprint database based on calibrated propagation model," *IEEE Trans. Instrum. Meas.*, vol. 68, no. 8, pp. 2714–2723, Aug. 2019.
[33] H. Zheng, Z. Xu, C. Yu, and M. Gurusamy, "A 3-D high accuracy positioning system based on visible light communication with novel positioning algorithm," *Opt. Commun.*, vol. 396, pp. 160–168, Aug. 2017.
[34] S. W. Ho, J. Duan, and C. S. Chen, "Location-based information transmission systems using visible light communications," *Trans. Emerg. Telecommun. Technol.*, vol. 28, no. 1, p. e2922, 2017.